Diameter dependence of TO phonon frequencies and the Kohn anomaly in armchair single-wall carbon nanotubes

Hagen Telg, Erik H. Hároz, Juan G. Duque, Xiaomin Tu, Constantine Y. Khripin, Jeffrey A. Fagan, Ming Zheng, Junichiro Kono, and Stephen K. Doorn

Phys. Rev. B **90**, 245422 — Published 15 December 2014

DOI: 10.1103/PhysRevB.90.245422

Diameter Dependence of TO Phonon Frequencies and the Kohn Anomaly in Armchair Single-Wall Carbon Nanotubes

Hagen Telg,[1,*] Erik H. Hároz,[1,2] Juan G. Duque,[3] Xiaomin Tu,[4] Constantine Y. Khripin,[4] Jeffrey A. Fagan,[4] Ming Zheng,[4] Junichiro Kono,[2] and Stephen K. Doorn[1,†]

[1] *Center for Integrated Nanotechnologies, Los Alamos National Laboratory, Los Alamos, New Mexico 87545, USA*
[2] *Department of Electrical and Computer Engineering, Rice University, Houston, Texas 77005, USA.*
[3] *Chemistry Division, Physical Chemistry and Applied Spectroscopy (C-PCS), Los Alamos National Laboratory, Los Alamos, New Mexico 87545, USA*
[4] *Materials Science and Engineering Division, National Institute of Standards and Technology, Gaithersburg, Maryland 20899, USA*

(Dated: November 24, 2014)

We present resonant Raman scattering experiments on nanotube samples enriched in metallic armchair single-wall carbon nanotubes (SWCNTs). We establish the transverse optical ($\mathcal{A}_{TO}$) phonon frequency for the (5,5) through (10,10) armchair species, ranging in diameter from 0.68 to 1.36 nm. The frequencies show a strong diameter dependence similar to that previously observed in semiconducting nanotubes. We show that the $\mathcal{A}_{TO}$ frequencies in armchair SWCNTs are dramatically upshifted from those of semiconducting SWCNTs. Furthermore, using electrochemical doping, we demonstrated that the $\mathcal{A}_{TO}$ frequencies in armchair SWCNTs are independent of the position of the Fermi level. These results suggest that the upshift is a result of a Kohn anomaly involving a forward-scattering mechanism of electrons close to the Fermi level. This is in contrast to the well-known Kohn anomaly that dominates the downshift of the $\mathcal{A}_{LO}$ and $\mathcal{E}_{2g}$ phonons in non-armchair metallic SWCNTs and graphene, respectively.

PACS numbers: 61.48.De, 63.22.Gh, 73.22-f, 78.30.Na, 78.67.Ch, 81.07.De

In recent years, strong progress in separation techniques has made SWCNT samples available that are purified with respect to nanotube diameter distribution, metallicity (metallic or semiconducting), chiral angle or even precise chirality (n,m).[1–10] Based on experiments performed on such samples, new physical phenomena were revealed the plasmon resonance origin of terahertz conductivity,[11] higher-order coherent phonon generation,[12] quantum interference,[13] and the breakdown of the Condon approximation.[14]

Raman spectroscopy has proven itself a valuable tool in SWCNT research, for routine characterization purposes as well as for the study of novel physical properties. The diameter dependence of some phonon modes, strong resonance enhancement of the Raman signal coupled with narrow resonance windows, and systematic variations in the electron-phonon coupling (EPC) allow the determination of SWCNT diameters, chiral angles, and even the exact atomic structure given by the chiral indices (n,m).[15–20] It has been shown that, when the resonance condition of non-armchair metallic nanotubes (SWCNT species where $\nu = (n-m) \mod 3 = 0$ and where $n \neq m$) is met, the G-mode shows a broad feature that can be used to identify metallic nanotubes and which later was assigned to a strong coupling of the longitudinal optical phonon to electrons close to the Fermi level, commonly known as a Kohn anomaly (KA).[21–26]

In the majority of SWCNT – all but (n,0) (zigzag) and (n,n) (armchair) tubes – the G-mode is composed of two Raman peaks, G^+ (higher energy) and G^- (lower energy), with frequencies between 1500 and 1600 cm^{-1}. The origin of these peaks are the fully symmetric transverse ($\mathcal{A}_{TO}$) and longitudinal ($\mathcal{A}_{LO}$) optical phonons, both related to the $\mathcal{E}_{2g}$ phonon in graphene. In semiconducting SWCNTs (S-SWCNTs), where $\nu = (n - m) \mod 3 \neq 0$, G^- is related to the $\mathcal{A}_{TO}$ ($\mathcal{A}^S_{TO}$) and G^+ to the $\mathcal{A}_{LO}$ ($\mathcal{A}^S_{LO}$) phonon, and dependences of both phonons on the various SWCNT parameters (diameter, chiral angle, *etc.*) and the involved photophysical processes are well-understood.[19] In metallic SWCNTs (M-SWCNTs), where $\nu = (n - m) \mod 3 = 0$, the order of the peaks is opposite with the $\mathcal{A}^M_{LO}$ phonon having a lower frequency than the $\mathcal{A}^M_{TO}$ phonon.[26,27] As mentioned above, the $\mathcal{A}^M_{LO}$ phonon is downshifted and broadened as a result of a Kohn anomaly. With respect to $\mathcal{A}^S_{TO}$, $\mathcal{A}^M_{TO}$ is upshifted. The origin of this upshift is still under debate, with two contradicting theoretical models. One model ascribes the upshift to an additional Kohn anomaly, which can only be observed in theoretical studies if the Born-Oppenheimer approximation is dropped.[26,28] The other model predicts the upshift of $\mathcal{A}^M_{TO}$ to be a result of the same Kohn anomaly as that in the $\mathcal{A}^M_{LO}$, however, involving a much weaker electron-phonon coupling.[29]

Besides the interest in resolving this controversy in the interpretation of the $\mathcal{A}^M_{TO}$ frequencies, there is significant interest in the exact frequencies of the $\mathcal{A}^M_{TO}$ and $\mathcal{A}^M_{LO}$ as a function of various SWCNT parameters for SWCNT characterization purposes. At present, such information is very limited due to the spectral overlap of signal from different (n,m) SWCNT species, which is a common issue when dealing with mixed chirality samples. Therefore, the only currently available data is based on experiments on individual tubes and limited to large-diameter nanotubes.[20,30,31] Furthermore, these previous

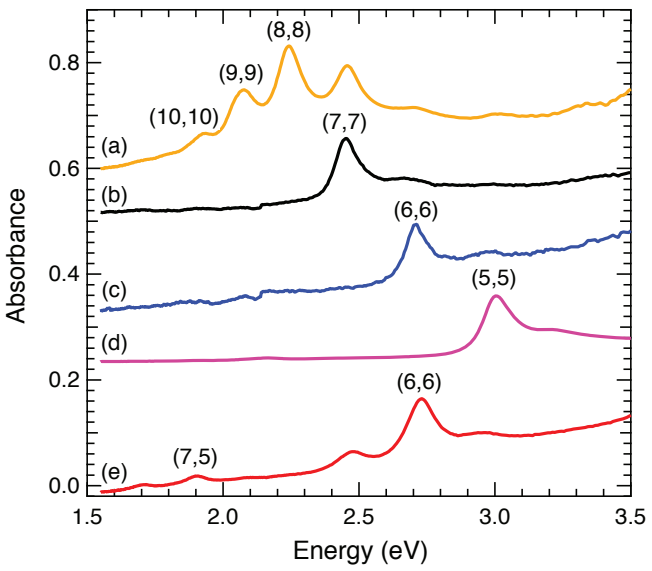

FIG. 1. Optical absorption spectra of aqueous 1% (wt./vol.) DOC solutions of armchair-enriched samples, prepared via DGU [(a)-orange trace], DNA-IEX [(b)-black and (c)-blue traces], and ATPE [(d)-magenta and (e)-red traces] methods. All spectra are offset and scaled for clarity.

studies have focused on the $\mathcal{A}_{LO}^{M}$ phonon, whose usefulness to determine structural properties of a particular M-SWCNT is questionable due to strong frequency variations with changes of the Fermi level. Given that the $\mathcal{A}_{TO}^{M}$ frequency is insensitive to changes in the Fermi level, the $\mathcal{A}_{TO}^{M}$ could become an additional characterization tool for M-SWCNTs similar to the $\mathcal{A}_{TO}^{S}$ phonon for S-SWCNTs.[19]

In this paper, we present resonant Raman scattering experiments on SWCNT samples, which are enriched in armchair chiralities, *i.e.* $n = m$. For the first time, a systematic dependence of the $\mathcal{A}_{TO}^{M}$ phonon frequency on nanotube diameter was observed. The frequencies are significantly higher than those in S-SWCNTs, indicating the presence of a Kohn anomaly. We show that variations in the Fermi level have only minor effects on the $\mathcal{A}_{TO}^{M}$ frequencies, which is consistent with a forward-scattering process being involved in the Kohn anomaly. This is in contrast to the Kohn anomaly in $\mathcal{A}_{LO}^{M}$ phonons, which involves a backscattering process.

I. EXPERIMENTAL

All samples used in this study were enriched in armchair SWCNTs and produced using the density gradient ultracentrifugation (DGU),[4,32] DNA-based anion-exchange chromatography (DNA-IEX),[5] or aqueous two-phase extraction (ATPE)[9] separation techniques as described in the noted references. Optical absorption spectra for the various samples are shown in Fig. 1. The DGU method provides an enrichment of armchair chiralities in general, showing enrichment in armchair species (6,6)-(10,10) for HiPco HPR 188.2 material [orange-(a) trace]. The DNA-IEX [black-(b) and blue-(c) traces] and ATPE [magenta-(d) trace] methods produce suspensions enriched in a single armchair species with namely (6,6) and (7,7) enriched via DNA-IEX and (5,5) via ATPE using CoMoCAT SG65 and SG65i material, respectively. Finally, ATPE was also used to generate a (6,6)-enriched sample from CoMoCAT SG65i material [absorption spectrum Fig. 1 (e), red trace] for preparation of an armchair-enriched thin film. After enrichment, all samples were dialyzed into aqueous 1% (wt./vol.) sodium deoxycholate (DOC) solutions to homogenize the environment surrounding the SWCNTs.

Raman scattering experiments were performed in backscattering geometry using excitation energies in resonance with the first optical transition, E_{11}^{M}, of the particular nanotube (see Table I) in question. Therefore, we utilized various excitation sources including an argon-ion laser, a dye laser pumping Rhodamine 6G, Rhodamine 110, or Kiton Red dyes, and the second harmonic of a Ti:Sapphire laser. Raman spectra were collected using a triple monochromator setup attached with a charge-coupled device detector. All spectra were frequency-calibrated using the Raman lines of 4-acetamidophenol or benzonitrile.[18]

To study the Raman signal of armchair SWCNTs as a function of Fermi level, we used the ATPE-produced CoMoCAT SG65i sample [Fig. 1 (e)] to produce a thin film by vacuum filtration.[34] We then transferred the film onto an ITO-coated glass slide, and constructed an electrochemical cell by gluing a spacer and a second ITO-coated glass slide to the first slide, leaving a volume which we filled with a 1M potassium chloride solution to achieve mild doping conditions (see device sketch in Fig. 5 (d)). Excitation and collection was done through the slide/ITO on which the film was deposited.

TABLE I. Summary of the studied armchair nanotubes (n,n).

(n,n)	d_t (nm)[a]	E_{11}^{M} (eV)[b]	ω(RBM) (cm^{-1})[c]	$\omega(\mathcal{A}_{TO}^{M})$ (cm^{-1})[d]	$\Gamma(\mathcal{A}_{TO}^{M})$ (cm^{-1})
(10,10)	1.36	1.93	174.3	1590.7	8.5
(9,9)	1.22	2.08	192.4	1590.3	9.0
(8,8)	1.09	2.24	216.4	1588.6	9.7
(7,7)	0.95	2.45	248.2	1585.9	8.8
(6,6)	0.81	2.71	287.5	1581.0	10.4
(5,5)	0.68	3.01	338.0	1573.5	12.9

[a] diameter $d_t = a_0\sqrt{n^2+nm+m^2}/\pi$, where $a_0 = 0.246$ nm is the in-plane lattice constant of graphite[33]
[b] Values were extracted from Fig. 1
[c] The experimental uncertainties for ω(RBM) for the (10,10); (9,9); (8,8); (7,7); (6,6); and (5,5) are ± 0.9, 0.8, 0.8, 0.8, 0.6 and 0.6 cm^{-1}, respectively.
[d] The experimental uncertainties for $\omega(\mathcal{A}_{TO}^{M})$ for the (10,10); (9,9); (8,8); (7,7); (6,6); and (5,5) are ± 0.9, 0.8, 0.8, 0.2, 0.6 and 0.6 cm^{-1}, respectively.

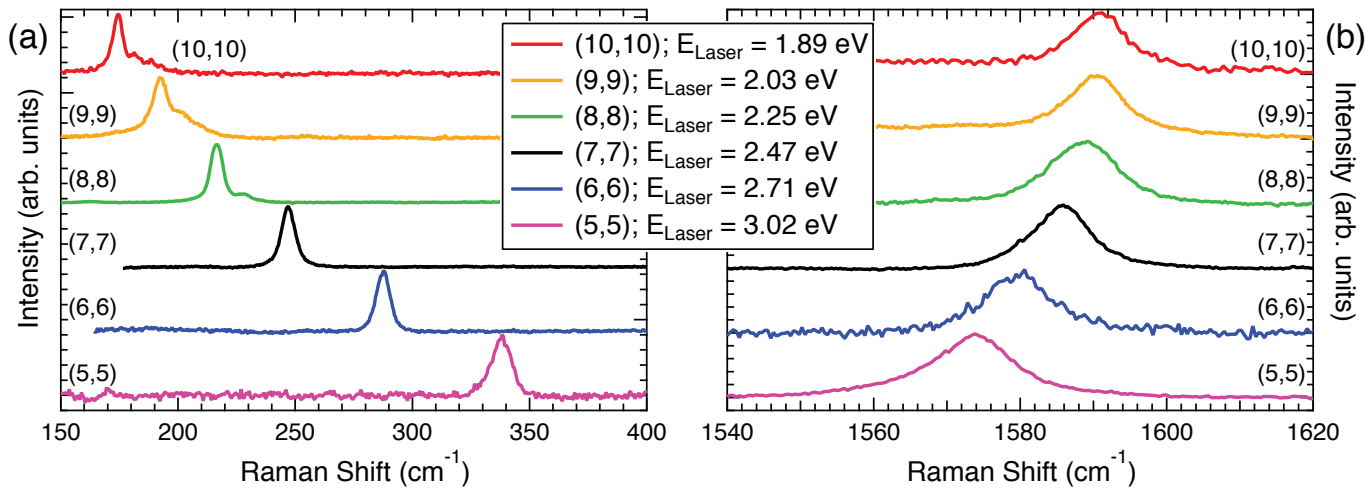

FIG. 2. (a) RBM and (b) G-mode spectra of the various samples in aqueous 1% (wt./vol.) DOC solution excited in resonance with the particular armchair SWCNT given in the legend. Excitation energies for both RBM and G-mode spectra for a given chirality are as indicated in the figure. For clarity, all spectra are normalized to the maximum peak intensity.

II. RESULTS AND DISCUSSION

Fig. 2 shows (a) the radial breathing mode (RBM) and (b) G-mode spectra obtained from aqueous 1% (wt./vol.) DOC solutions of the various samples. Each spectrum was collected exciting resonantly into the first optical transition, E_{11}^M, of the particular armchair nanotube given in the legend of the two figures. All spectra, G-mode as well as RBM, show a single dominant peak indicating that primarily one nanotube chirality (n,m) is in resonance at the particular excitation energy. By correlating the RBM frequency to the optical transition energy, all RBMs, and therefore the SWCNTs in resonance, can be assigned to chiralities with $\nu = 0$ (*i.e.* metallic SWCNTs).[16] It is well-known that the $\mathcal{A}_{LO}^M$ phonon is strongly broadened and softened due to a Kohn anomaly resulting in peak widths of > 50 cm^{-1}.[20,25] G-modes observed in our study have peak widths of ~ 10 cm^{-1} (see Table I). The correlation of an assignment to metallic nanotubes and the observation of a narrow peak width leads us to conclude that the observed peaks originate from the $\mathcal{A}_{TO}^M$ phonon of metallic nanotubes (consistent with findings in Ref. 5 and 35). Since the G-mode spectra show almost no sign of the downshifted and broadened $\mathcal{A}_{LO}^M$ phonon, we can assign the observed G-modes to the $\mathcal{A}_{TO}^M$ phonons of armchair carbon nanotubes in which $\mathcal{A}_{LO}^M$ phonons are not Raman-active.[5,20,35–37]

In order to study the Raman shift/phonon frequency (ω) of armchair SWCNTs as a function of nanotube diameter (d_t), we fit all observed peaks with Lorentzian functions. Along with relevant nanotube parameters, fit results for ω are summarized in Table I. Fig. 3 shows the observed $\mathcal{A}_{TO}^M$ phonon frequencies, $\omega(\mathcal{A}_{TO}^M)$, as a function of the nanotube diameter. In addition, we plotted the G^- and G^+ peak positions, $\omega(\mathcal{A}_{TO}^S)$ and $\omega(\mathcal{A}_{LO}^S)$, for semiconducting nanotubes taken from Ref. 19 and 38. Frequencies $\omega(\mathcal{A}_{TO}^M)$ in armchair nanotubes clearly distinguish themselves from $\omega(\mathcal{A}_{TO}^S)$ and $\omega(\mathcal{A}_{LO}^S)$. Most notably, for all diameters $\omega(\mathcal{A}_{TO}^M)$ is significantly higher than $\omega(\mathcal{A}_{TO}^S)$. In fact, for nanotubes with diameter $d_t > 1$ nm, $\omega(\mathcal{A}_{TO}^M)$ is very similar to $\omega(\mathcal{A}_{LO}^S)$. This similarity in $\mathcal{A}_{TO}^M$ and $\mathcal{A}_{LO}^S$ frequencies imposes a large uncertainty in the (n,m) assignment of individual SWCNTs and for determining if the SWCNT is a single tube or a small bundle, respectively.[20,25] In the case of smaller diameter ($d_t < 1$ nm) nanotubes, a more pronounced diameter dependence of $\omega(\mathcal{A}_{TO}^M)$ compared to $\omega(\mathcal{A}_{LO}^S)$ results in these two peaks being distinguishable.

TABLE II. Results from fitting Eqn. 1 to data from this work and data published in the given references. $\mathcal{A}_{TO}^M$, $\mathcal{A}_{TO}^S$, and $\mathcal{A}_{LO}^S$ name the TO phonons in armchair SWCNTs and TO and LO phonons in semiconducting (S) SWCNTs, respectively.

Ref.	a_0	a_1	a_2
$\mathcal{A}_{TO}^M$ (this work)	1582	-24.0 ± 0.6	29.3 ± 0.8
$\mathcal{A}_{TO}^S$ (expt.)[a]	1582	-27.5	0
$\mathcal{A}_{LO}^S$ (expt.)[a]	1582	-14.9	24.9
$\mathcal{A}_{TO}^M$ (theor.)[b]	1580.8	0	24.8

[a] Ref. 19
[b] Fit to data from Ref. 26. Note, curvature and thus rehybridization are not considered.

We fitted $\omega(\mathcal{A}_{TO}^M)$ with the empirical expression suggested in Ref. 19,

$$\omega_{\mathcal{A}_{TO}^M}(d_t) = a_0 + \frac{a_1}{d_t^2} + \frac{a_2}{d_t} \qquad (1)$$

and obtained excellent agreement with the two-parameter model. Here, a_0 is fixed to 1582 cm^{-1}, the frequency of the $\mathcal{E}_{2g}$ phonon of freestanding graphene, which resembles the limit of Eq. 1 for infinitely large

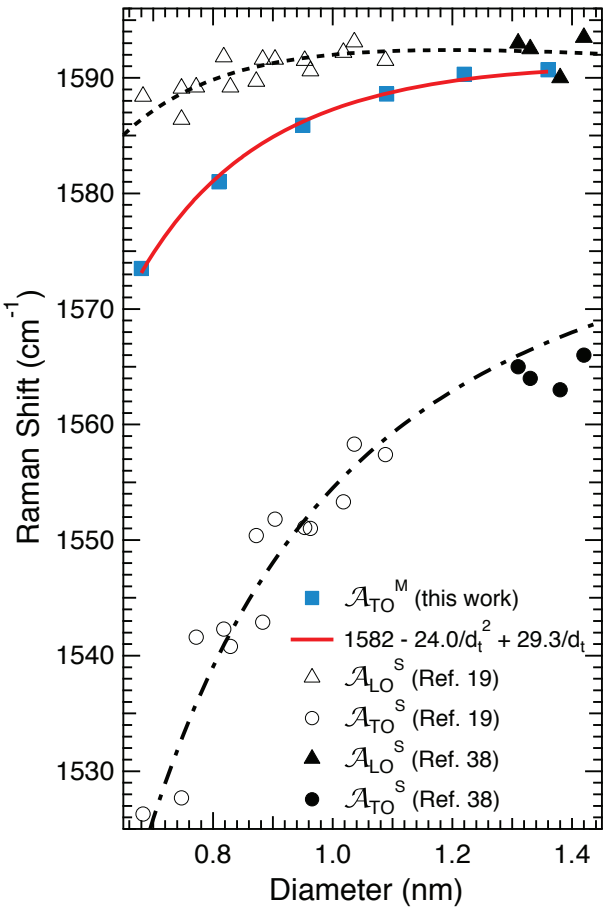

FIG. 3. $\mathcal{A}_{TO}^{M}$ frequency (blue squares) and its fit to Eqn. 1 (solid line) as a function of diameter. Below $\approx$ 1 nm $\mathcal{A}_{TO}^{M}$ can clearly be distinguished from the LO ($\mathcal{A}_{LO}^{S}$, triangles) and TO ($\mathcal{A}_{TO}^{S}$, circles) phonons in semiconducting SWCNT (taken from Ref. 19 and 38). Fits to Eqn. 1 for $\mathcal{A}_{LO}^{S}$ and $\mathcal{A}_{TO}^{S}$ are shown as dashed and dashed-dotted lines, respectively, using the parameters given in Table II.

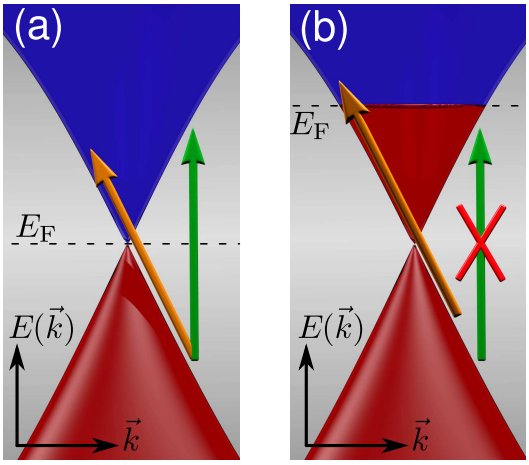

FIG. 4. An illustration of how variations in the Fermi energy, E_F, affect a Kohn anomaly involving a backscattering of electrons (green vertical arrow), where $\partial E(k)/\partial k$ changes sign, and a forward-scattering process (orange diagonal arrow), where no sign change in $\partial E(k)/\partial k$ occurs. (a) and (b) show the electronic band structure of a semimetal with linear bands equivalent to that of metallic SWCNTs. In (a), the undoped case, both processes are possible. In (b), as E_F is changed by more than half the phonon energy, the backscattering process is blocked while the forward-scattering remains possible.

diameter nanotubes.[39,40] For semiconducting nanotubes, we showed in Ref. 19 that the second term in Eqn. 1 is related to the rehybridization of sp^2 to sp^3 orbitals. The finding of very similar values of a_1 for $\mathcal{A}_{TO}^{M}$ ($a_1 = -24.0$) and $\mathcal{A}_{TO}^{S}$ ($a_1 = -27.5$) indicates that phonon frequencies in metallic nanotubes are affected by rehybridization in the same way as semiconducting tubes.

For semiconducting nanotubes, it was shown that the third term in Eqn. 1, a_2/d_t, is related to confinement effects, which affect $\mathcal{A}_{LO}$ phonons only. The term in this work ($a_2 = +29.3$), which results in a dramatic upshift of the $\mathcal{A}_{TO}^{M}$ frequencies compared to the $\mathcal{A}_{TO}^{S}$, must be of a different origin. It is well-known that frequency and lifetime of $\mathcal{A}_{LO}^{M}$ phonons are strongly affected by a KA.[22–24] The origin of this KA can be found in the strong EPC of $\mathcal{A}_{LO}^{M}$ phonons to electrons close to the Fermi level, which results in the creation of electron-hole pairs that damp the phonons and subsequently reduce their lifetimes (see illustration in Fig. 4). The $\mathcal{A}_{TO}^{M}$ phonons, on the other hand, are expected to be less affected by a similar transition because of a much weaker EPC. Ref. 29 predicts that in some cases a weak coupling can result in an upshift of the $\mathcal{A}_{TO}^{M}$ frequency. However, a non-zero EPC is only expected for narrow band gap "metallic tubes". Armchair tubes – the chiralities studied in this work – are the only metallic tubes which are truly metallic and therefore have no band gap.[41,42] Based on our finding, the theory presented in Ref. 29 would suggest that armchair SWCNTs have a small band gap. In this case, Ref. 29 predicts a dependence of the $\mathcal{A}_{TO}^{M}$ frequency with changes in the Fermi level.

Alternatively, Piscanec *et al.* predict that theoretical descriptions of phonons in metallic nanotubes that are based on an adiabatic approximation are inaccurate.[26] By describing phonons as time-dependent perturbations of the system, Piscanec *et al.* included dynamic effects, which in some cases, dramatically affect phonon frequencies. With respect to our work, the most significant result from Ref. 26 is the prediction of a new (third) Kohn anomaly in the phonon dispersion of metallic nanotubes. Along with the established KAs in the $\mathcal{A}_{LO}^{M}$ and $\mathcal{A}_{TO}^{M}$ phonon dispersions close to the Γ-point and the K-point, respectively, they predicted an additional KA for $\mathcal{A}_{TO}^{M}$ close to the Γ-point. While the KA for $\mathcal{A}_{LO}^{M}$ is related to a backscattering process (green arrow in Fig. 4 (a)), the Γ-point KA in $\mathcal{A}_{TO}^{M}$ is related to a forward scattering process (orange arrow in Fig. 4 (a)).[43] From Fig. 4, it is obvious that forward-scattering in-

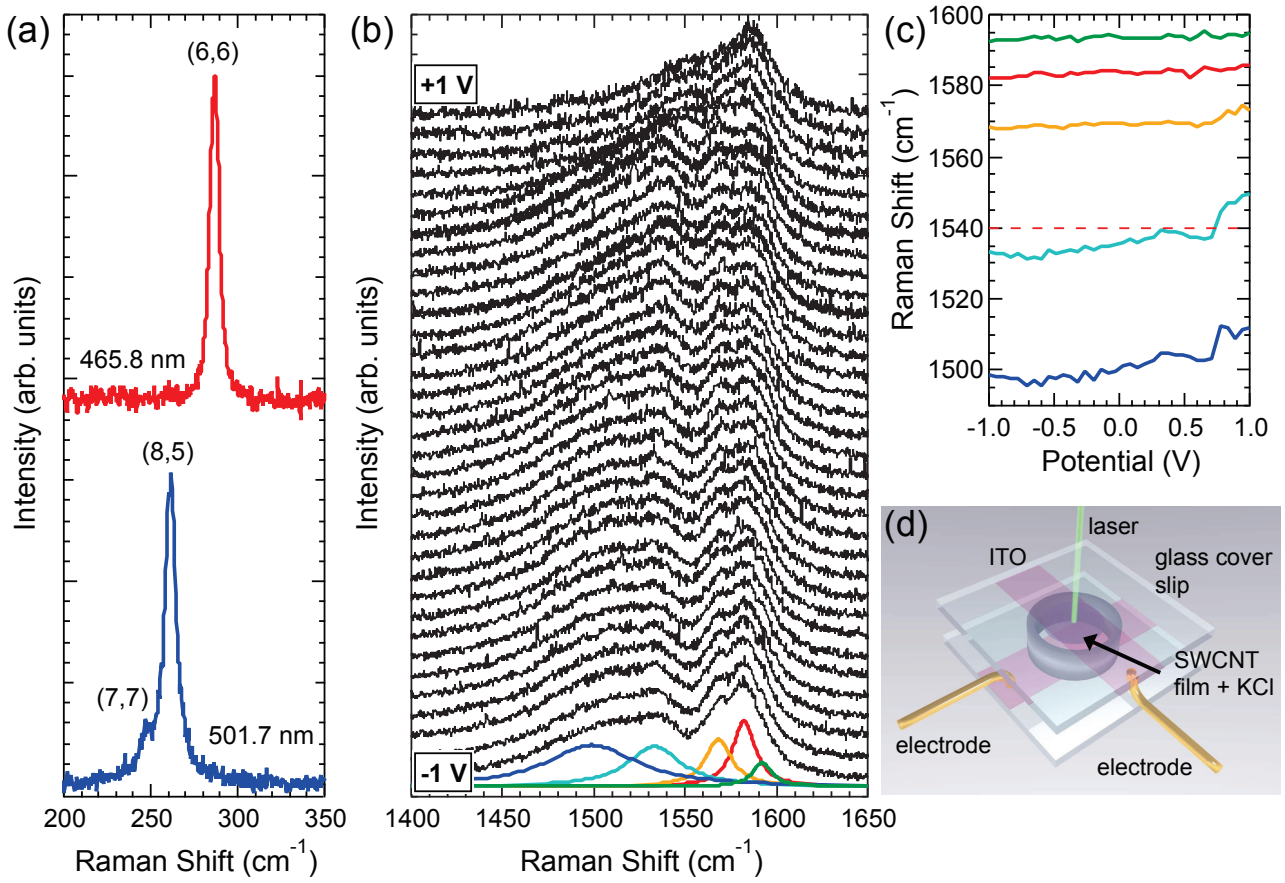

FIG. 5. (a) RBM spectra with excitation at 465.8 nm (top) and 501.7 nm (bottom) of the (6,6)-enriched thin film used for electrochemical doping. (b) G-band spectra of a (6,6)-enriched thin film as a function of electrochemical potential taken at 465.8 nm laser excitation. Potential is varied from -1 V (bottom) to +1 V (top), in 55 mV steps. Spectra were decomposed into 5 Lorentzian components labelled blue (1498 cm^{-1}), cyan (1532 cm^{-1}), orange (1567 cm^{-1}), red (1582 cm^{-1}), and green (1592 cm^{-1}), where the noted peak positions are taken from the spectrum measured at V = -1 V. (c) Peak positions of the 5 Lorentzian components fitted to the spectra in Fig. 5(b) as a function of electrochemical potential. Dashed line indicates the 1540 cm^{-1} expected $\mathcal{A}_{LO}^{S}$ frequency for semiconducting species of the same diameter as the (6,6). (d) A schematic diagram of the electrochemical cell used to measure spectra in Fig. 5 (b).

volves non-Γ-point phonons and therefore should not influence Raman signal. However, the intensity of the KA in combination with the broadening of the involved electronic states would result in an upshift of Γ-point $\mathcal{A}_{TO}^{M}$ phonons by tens of cm^{-1}.[26,28] The backscattering process can be Pauli-blocked by changing the Fermi level (unoccupied states into which electrons could be scattered by the phonons are no longer available). However, only extreme doping levels – doping beyond the linear regime of the electronic bands – are expected to have an effect on the forward-scattering process. In other words, changes in the Fermi level neither affect the availability of states into which an electron can be scattered by the particular phonon, nor does it lead to a change of the wavevector and consequently the energy of the scattered phonon due to the linearity of the electronic bands (see illustration in Fig. 4). Assuming the upshift of the $\mathcal{A}_{TO}^{M}$ phonon in armchair carbon nanotubes to be exclusively related to the KA involving the forward-scattering process, no changes in frequency or linewidth should be observed when moderately shifting the Fermi level.[44]

We note the anticipated $\mathcal{A}_{TO}^{M}$ upshift of Ref. 26 yields for Eqn. 1 a predicted a_2 value of 24.8 (Table II), consistent with our experimental value of 29.3 and suggestive of the forward-scattering process. In order to further determine which of the two mechanisms – a finite band gap in armchair SWCNTs or a novel KA involving forward-scattering of electrons – is responsible for the significant upshift of the $\mathcal{A}_{TO}^{M}$ frequency compared to the $\mathcal{A}_{TO}^{S}$ frequency, we varied the Fermi level by electrochemically doping a thin film of the (6,6) armchair-SWCNT-enriched sample. As seen in the absorption spectrum of the source material for the (6,6)-enriched film [Fig. 1 (e)], the sample is highly-enriched in (6,6) but also contains other metallic impurity species of the (7,7) family of tubes (feature at 2.48 eV), as well as some

small semiconducting nanotube contaminants (e.g., feature at 1.9 eV). RBM spectra of the film are shown in Fig. 5 (a). With excitation at 465.8 nm (resonant with the (6,6) absorption), only the (6,6) RBM feature is observed. Excitation at 501.7 nm (resonant with the (7,7) family of metallic structures) shows that both (7,7) and (8,5) species are present at low levels as well. Fig. 5 (b) shows G-mode Raman spectra from the nanotube film enriched in (6,6) armchair SWCNTs. All spectra were excited at a wavelength of 465.8 nm. The potential applied to the electrochemical cell varied from -1 to 1 V, as shown from bottom to top in Fig. 5 (b). Because of the contamination in the sample from impurity species (discussed above), five peaks are observed in the measured spectra. These are fit well with five Lorentzian lineshapes and are assigned as follows.

The feature of interest here is the peak at 1582 cm^{-1}, which can be assigned to the $\mathcal{A}_{TO}^{M}$ of the (6,6) nanotube, based on frequency and linewidth. Given the diameter distribution of the source material, 0.62-1.10 nm with average diameter of 0.76 nm, the results of Fig. 3 further rule out semiconducting tubes as the source of this peak. Likewise, within this diameter range, the peak at 1567 cm^{-1} cannot originate from an $\mathcal{A}_{TO}$ or $\mathcal{A}_{LO}$ phonon for any feasible metallic or semiconducting species. This mode is likely a normally forbidden $\mathcal{E}$-symmetry mode that becomes allowed as a result of intertube interactions present in the bundled film.[27] The remaining peaks can be attributed to (n,m) contamination. The broad peaks at 1498 cm^{-1} and at 1532 cm^{-1} (at V = -1 V) indicate some presence of non-armchair metallic nanotubes (further supported by the observation of the (8,5) RBM) and are associated with the $\mathcal{A}_{TO}^{M}$ phonon in such tubes. The peak at 1592 cm^{-1} is present as a small shoulder at higher frequency and may be assigned as the $\mathcal{A}_{LO}$ contribution from semiconducting impurities. Given the relative weakness of this $\mathcal{A}_{LO}^{S}$ contribution to the spectrum, it is not surprising that a corresponding $\mathcal{A}_{TO}^{S}$ is not apparent. In summary, we thus note that the G-band spectra obtained from the thin film are more highly featured than those observed from aqueous suspensions of the film's source material. We attribute this to the symmetry breaking and broadening of electronic resonances resulting from intertube interactions that occur with nanotube bundle formation within the film.[27,45] Ideally, our film would be free of these (n,m) contaminants, but their presence yields an advantage for validation of the observed (6,6) response on varying the applied potential.

In Fig. 5 (c), we show the evolution of the peak positions as a function of applied potential. As expected and previously demonstrated, the $\mathcal{A}_{LO}^{M}$ peak shows an upshift with increasing potential ($\omega|_{-1\,\mathrm{V}}$ = 1498 and 1532 cm^{-1}), and decreasing intensity, indicating that the backscattering mechanism becomes blocked.[22–24] The $\mathcal{A}_{TO}^{M}$ of (6,6) SWCNTs, however, is mostly unaffected by changes in the potential. This result clearly favors the interpretation of an additional KA involving a forward-scattering mechanism as the process leading to the upshift of $\mathcal{A}_{TO}^{M}$ phonon frequencies.[26,44] If the origin of the upshift would be a KA similar to that of the $\mathcal{A}_{LO}^{M}$ phonons, we would have expected the frequency of the $\mathcal{A}_{TO}^{M}$ mode to approach $\sim$ 1540 cm^{-1}, which is the $\mathcal{A}_{TO}^{S}$ phonon frequency of similar diameter semiconducting nanotubes [dashed line in Fig. 5 (c)].[19,46]

In conclusion, we present Raman scattering experiments on armchair SWCNTs (5,5)-(10,10) with diameters between 0.68 nm and 1.36 nm, respectively. For nanotubes smaller than 1 nm, the $\mathcal{A}_{TO}$ phonon mode in armchairs can clearly be distinguished from modes in semiconductors. We find that the frequency of $\mathcal{A}_{TO}$ phonons in armchair SWCNTs is independent of moderate variations in the Fermi level – variations which do not lead to injections of charges into higher electronic bands. This makes the $\mathcal{A}_{TO}$ phonon an excellent tool to determine the metallicity and diameter of small-diameter SWCNTs. The finding of a Fermi level independence of the $\mathcal{A}_{TO}$ frequency allows us to determine the process that results in the upshift of the $\mathcal{A}_{TO}$ phonon in armchair SWCNTs compared to semiconducting SWCNTs. Our results are consistent with a Kohn anomaly involving a forward-scattering of electrons close to the Fermi level, which therefore distinguishes itself from the Kohn anomaly in $\mathcal{A}_{LO}$ phonons in non-armchair metallic SWCNTs and the $\mathcal{E}_{2g}$ phonon in graphene.

ACKNOWLEDGMENTS

H.T., E.H.H., J.G.D., and S.K.D. acknowledge support of the LANL-LDRD program. H.T. and E.H.H. also gratefully acknowledge support from the LANL Director's Postdoctoral Fellowship. E.H.H. and J.K. were supported by the DOE/BES through Grant DEFG02-06ER46308 and the Robert A. Welch Foundation through Grant C-1509. This work was performed in part at the Center for Integrated Nanotechnologies, a U. S. Department of Energy, Office of Basic Energy Sciences user facility. Certain equipment, instruments or materials are identified in this paper in order to adequately specify the experimental details. Such identification does not imply recommendation by the authors nor does it imply the materials are necessarily the best available for the purpose.

* Current address: *Chemical Sciences Division, NOAA Earth System Research Laboratory and USA Cooperative Institute for Research in Environmental Sciences, University of Colorado-Boulder, Boulder, Colorado 80305, USA*

† Corresponding author email: *skdoorn@lanl.gov*

[1] R. Krupke, F. Hennrich, H. von Lohneysen, and M. M. Kappes, Science **301**, 344 (2003).

[2] M. S. Arnold, A. A. Green, J. F. Hulvat, S. I. Stupp, and M. C. Hersam, Nature Nanotechnol. **1**, 60 (2006).

[3] X. Tu, S. Manohar, A. Jagota, and M. Zheng, Nature **460**, 250 (2009).

[4] E. H. Hároz, W. D. Rice, B. Y. Lu, S. Ghosh, R. H. Hauge, R. B. Weisman, S. K. Doorn, and J. Kono, ACS Nano **4**, 1955 (2010).

[5] X. Tu, A. R. Hight Walker, C. Y. Khripin, and M. Zheng, J. Am. Chem. Soc. **133**, 12998 (2011).

[6] H. Liu, D. Nishide, T. Tanaka, and H. Katuara, Nat. Commun. **2**, 309 (2011).

[7] K. S. Mistry, B. A. Larsen, and J. L. Blackburn, ACS Nano **7**, 2231 (2013).

[8] C. Y. Khripin, J. A. Fagan, and M. Zheng, J. Am. Chem. Soc. **135**, 6822 (2013).

[9] J. A. Fagan, C. Y. Khripin, C. A. S. Batista, J. R. Simpson, E. H. Hároz, A. R. H. Walker, and M. Zheng, Adv. Mater. **26**, 2800 (2014).

[10] N. K. Subbaiyan, S. Cambré, A. N. G. Parra-Vasquez, E. H. Hároz, S. K. Doorn, and J. G. Duque, ACS Nano **8**, 1619 (2014).

[11] Q. Zhang, E. H. Hároz, Z. Jin, L. Ren, X. Wang, R. S. Arvidson, A. Lüttge, and J. Kono, Nano Lett. **13**, 5991 (2013).

[12] Y.-S. Lim, A. R. T. Nugraha, S.-J. Cho, M.-Y. Noh, E.-J. Yoon, H. Liu, J.-H. Kim, H. Telg, E. H. Hároz, G. D. Sanders, S.-H. Baik, H. Kataura, S. K. Doorn, C. J. Stanton, R. Saito, J. Kono, and T. Joo, Nano Lett. **14**, 1426 (2014).

[13] J. G. Duque, H. Telg, H. Chen, A. K. Swan, A. P. Shreve, X. Tu, M. Zheng, and S. K. Doorn, Phys. Rev. Lett. **108**, 117404 (2012).

[14] J. G. Duque, H. Chen, A. K. Swan, A. P. Shreve, S. Kilina, S. Tretiak, X. Tu, M. Zheng, and S. K. Doorn, ACS Nano **5**, 5233 (2011).

[15] H. Telg, J. Maultzsch, S. Reich, F. Hennrich, and C. Thomsen, Phys. Rev. Lett. **93**, 177401 (2004).

[16] J. Maultzsch, H. Telg, S. Reich, and C. Thomsen, Phys. Rev. B **72**, 205438 (2005).

[17] C. Fantini, A. Jorio, M. Souza, M. S. Strano, M. S. Dresselhaus, and M. A. Pimenta, Phys. Rev. Lett. **93**, 147406 (2004).

[18] S. K. Doorn, D. A. Heller, P. W. Barone, M. L. Usrey, and M. S. Strano, Appl. Phys. A **78**, 1147 (2004).

[19] H. Telg, J. G. Duque, M. Staiger, X. Tu, F. Hennrich, M. M. Kappes, M. Zheng, J. Maultzsch, C. Thomsen, and S. K. Doorn, ACS Nano **6**, 904 (2012).

[20] T. Michel, M. Paillet, D. Nakabayashi, M. Picher, V. Jourdain, J. C. Meyer, A. A. Zahab, and J.-L. Sauvajol, Phys. Rev. B **80**, 245416 (2009).

[21] H. Kataura, Y. Kumazawa, Y. Maniwa, I. Umezu, S. Suzuki, Y. Ohtsuka, and Y. Achiba, Synthetic Metals **103**, 2555 (1999).

[22] J. C. Tsang, M. Freitag, V. Perebeinos, J. Liu, and P. Avouris, Nat. Nanotechnol. **2**, 725 (2007).

[23] K. T. Nguyen, A. Gaur, and M. Shim, Phys. Rev. Lett. **98**, 145504 (2007).

[24] H. Farhat, H. Son, G. G. Samsonidze, S. Reich, M. S. Dresselhaus, and J. Kong, Phys. Rev. Lett. **99**, 145506 (2007).

[25] M. Fouquet, H. Telg, J. Maultzsch, Y. Wu, B. Chandra, J. Hone, T. F. Heinz, and C. Thomsen, Phys. Rev. Lett. **102**, 075501 (2009).

[26] S. Piscanec, M. Lazzeri, J. Robertson, A. C. Ferrari, and F. Mauri, Phys. Rev. B **75**, 035427 (2007).

[27] O. Dubay, G. Kresse, and H. Kuzmany, Phys. Rev. Lett. **88**, 235506 (2002).

[28] V. N. Popov and P. Lambin, Nano Research **3**, 822 (2010).

[29] K. Sasaki, R. Saito, G. Dresselhaus, M. S. Dresselhaus, H. Farhat, and J. Kong, Phys. Rev. B **77**, 245441 (2008).

[30] A. Jorio, A. G. Souza Filho, G. Dresselhaus, M. S. Dresselhaus, A. K. Swan, M. S. Ünlü, B. B. Goldberg, M. A. Pimenta, J. H. Hafner, C. M. Lieber, and R. Saito, Phys. Rev. B **65**, 155412 (2002).

[31] M. Oron-Carl, F. Hennrich, M. M. Kappes, H. v. Löhneysen, and R. Krupke, Nano Lett. **5**, 1761 (2005).

[32] E. H. Hároz, J. G. Duque, B. Y. Lu, P. Nikolaev, S. Arepalli, R. H. Hauge, S. K. Doorn, and J. Kono, J. Am. Chem. Soc. **134**, 4461 (2012).

[33] Y. Baskin and L. Meyer, Phys. Rev. **100**, 544 (1955).

[34] B. Dan, A. W. K. Ma, E. H. Hároz, J. Kono, and M. Pasquali, Ind. Eng. Chem. Res. **51**, 10232 (2012).

[35] E. H. Hároz, J. G. Duque, W. D. Rice, C. G. Densmore, J. Kono, and S. K. Doorn, Phys. Rev. B **84**, 121403(R) (2011).

[36] M. Damnjanović, I. Milošević, T. Vuković, and R. Sredanović, Phys. Rev. B **60**, 2728 (1999).

[37] Y. Wu, J. Maultzsch, E. Knoesel, B. Chandra, M. Huang, M. Y. Sfeir, L. E. Brus, J. Hone, and T. F. Heinz, Phys. Rev. Lett. **99**, 027402 (2007).

[38] M. Paillet, T. Michel, J. C. Meyer, V. N. Popov, L. Henrard, S. Roth, and J.-L. Sauvajol, Phys. Rev. Lett. **96**, 257401 (2006).

[39] S. Reich, C. Thomsen, and J. Maultzsch, *Carbon Nanotubes: Basic Concepts and Physical Properties* (Wiley-VCH, Weinheim, 2004).

[40] S. Berciaud, S. Ryu, L. E. Brus, and T. F. Heinz, Nano Lett. **9**, 346 (2009).

[41] C. L. Kane and E. J. Mele, Phys. Rev. Lett. **78**, 1932 (1997).

[42] N. Hamada, S. Sawada, and A. Oshiyama, Phys. Rev. Lett. **68**, 1579 (1992).

[43] V. N. Popov and P. Lambin, Phys. Rev. B. **74**, 075415 (2006).

[44] V. N. Popov, Physica E: Low-Dimensional Systems and Nanostructures **44**, 1032 (2012).

[45] M. J. O'Connell, S. Sivaram, and S. K. Doorn, Phys. Rev. B **69**, 235415 (2004).

[46] J. S. Park, K. Sasaki, R. Saito, W. Izumida, M. Kalbac, H. Farhat, G. Dresselhaus, and M. S. Dresselhaus, Phys. Rev. B **80**, 081402 (2009).